

# Initial Shock Waves for Explosive Nucleosynthesis in Type II Supernova

Shigehiro NAGATAKI,<sup>1</sup> Masa-aki HASHIMOTO,<sup>2</sup> and Shoichi YAMADA<sup>1,3</sup>

<sup>1</sup> *Department of Physics, School of Science, the University of Tokyo, 7-3-1 Hongo, Bunkyo-ku, Tokyo 113*

*E-mail(TY): Nagataki@utaphp1.phys.s.u-tokyo.ac.jp*

<sup>2</sup> *Department of Physics, Faculty of Science, Kyusyu University, Ropponmatsu, Fukuoka 810*

<sup>3</sup> *Max-Planck-Institute für Physik und Astrophysik, Karl-Schwarzschild Strasse 1, D-8046, Garching bei München, Germany*

(Received 1997 June 20; accepted 1997 December 2)

## Abstract

We have performed 1-dimensional calculations for explosive nucleosynthesis in collapse-driven supernova and investigated its sensitivity to the initial form of the shock wave. We have found the tendency that the peak temperature becomes higher around the mass cut if the input energy is injected more in the form of kinetic energy rather than internal energy. Then, the mass cut becomes larger, and, as a result, neutron-rich matter is less included in the ejecta; this is favorable for producing the observational data compared with a previous model. Our results imply that the standard method to treat various processes for stellar evolution, such as convection and electron capture during the silicon burning stage, are still compatible with the calculation of explosive nucleosynthesis.

**Key words:** Nucleosynthesis — Supernovae: general — Supernovae: individual (SN 1987A)

## 1. Introduction

Elements heavier than  $^{12}\text{C}$  are mainly synthesized during the hydrostatic evolution of stars and supernova explosions. It can be said that massive stars play an important role concerning the chemical evolution of the Galaxy,

because they produce most elements of  $Z < 30$ . Until today, many calculations about stellar evolution and supernova explosion have been performed, and the compositions in the ejecta have been predicted. However, consistent calculations from stellar evolution to explosions still do not exist (e.g., Arnett 1996). In this paper we pay attention to collapse-driven supernova, which is regarded as the death of a massive star whose main sequence mass exceeds 8-times the solar mass ( $M_{\odot}$ ) (e.g., Hashimoto 1995).

Because of uncertainty concerning the collapse-driven supernova mechanism, calculations of stellar evolution and explosive nucleosynthesis during a supernova explosion have been done separately; a shock wave is artificially generated at the inner region of the core of the progenitor (Hashimoto et al. 1989).

Historically speaking, there have been two ways to generate a shock wave, as analyzed in detail by Aufderheide et al. (1991). One is called an internal-energy bomb (hereafter referred to as the bomb); the other is called a piston. In the approach of the bomb, the input energy is deposited in the form of internal energy at the inner-most edge of the calculation region, so that all of the energy deposited propagates outward. On the other hand, in the piston method, the inner-most edge is moved as a piston, so that the final explosion energy amounts to about  $10^{51}$  erg (Woosley, Weaver 1995).

Though these methods may be a good approximation, and explain many observational data, they have difficulty concerning the peak temperature during the early phase of the shock. Aufderheide et al. (1991) studied both the bomb and the piston methods to determine the influence on the initiation and propagation of the shock wave. They also investigated the effect due to the different launching time of the shock wave: at  $t = 0$  (the initial presupernova model: uncollapsed model) and after 0.28 s of core collapse (collapsed model). They found that up to a 10% difference in the major abundances from the different shock initiation schemes (the bomb or the piston) and up to 30% due to a variation in the launching time. The main result of their investigation is that the peak temperatures are different between the two methods in the early phase of shock propagation, although they converge as the shock waves propagate forward. This is because too much energy is deposited in the internal energy for the bomb and too much in the kinetic energy for the piston. As a result, there is uncertainty concerning the chemical composition in the inner region of the ejecta of  $M < 2M_{\odot}$ , whose progenitor mass is assumed to be a  $20 M_{\odot}$  star.

We now make an important comment concerning the presupernova model. Aufderheide et al. used the  $6 M_{\odot}$  helium-core model of Nomoto and Hashimoto (1988), which may have a problem of excessive neutronization. During the silicon burning, neutronization occurs below the O-rich layer due to electron capture. In this model some products

of explosive nucleosynthesis become too neutron-rich. For example, the ratio of the mass fraction  $^{58}\text{Ni}/^{56}\text{Ni}$  becomes much higher than the observation of SN 1987A (e.g., Hashimoto 1995).

Considering the large uncertainty of convective theory, Hashimoto (1995), including Aufderheide et al., have made the value of  $Y_e$  higher artificially in the Si-rich layer, so as to reproduce the observational ratios of the mass fraction for important nuclei, such as  $^{57}\text{Ni}/^{56}\text{Ni}$  and  $^{58}\text{Ni}/^{56}\text{Ni}$ . This means that the convection and/or the electron capture are limited in the Si-rich layer, and that the treatments of the convection and the electron capture during stellar evolution are inconsistent with the calculations of explosive nucleosynthesis because the discontinuity of  $Y_e$  in the progenitor is formed at the outer boundary of the convective shell (Thielemann et al. 1990; Hashimoto 1995). For example, the value of  $Y_e$  for  $M > 1.607M_\odot$  ( $=0.494$ ) is artificially changed to that of  $M > 1.637M_\odot$  ( $=0.499$ ) in Hashimoto (1995). We also note that the Schwarzschild criterion is adopted in Nomoto & Hashimoto (1988) for convective stability, neglecting both of overshooting and semiconvection, which means that the convective motion is fairly suppressed in the calculation of the progenitor.

In this paper, reversing the argument, we make use of the fact that the product of the explosive nucleosynthesis has uncertainty due to the poorly known initial form of the shock wave, and investigate whether we can find an initial shock wave which reproduces the observational data with the presupernova model unchanged. In particular, Aufderheide et al. (1991) studied only the bomb or the piston, and did not examine their combination. In this paper we show that an initial shock wave comprising a proper combination of kinetic and internal energy can reproduce the observed chemical abundances. This means that the electron-capture rates of Fuller et al. (1980, 1982) and convection using the Schwarzschild criterion during stellar evolution are still compatible with the observational data of the explosive nucleosynthesis products. Moreover, the form of the initial shock wave found in this study should be the outcome of core-collapse calculations.

In section 2 we explain explosive nucleosynthesis in a collapse-driven supernova explosion. In section 3, the methods adopted to calculate the explosive nucleosynthesis are described. We show the results in section 4. A summary is presented in section 5.

## 2. Explosive Nucleosynthesis

### 2.1. General Feature

In this section we give the general features of explosive nucleosynthesis that are common to collapse-driven supernova phenomena. The temperature and entropy per nucleon become high after the passage of a shock wave. The increase in temperature  $T$  causes various nuclear reactions that have been blocked by the Coulomb barrier in the nuclear burning stage during the hydrostatic stellar evolution. On the other hand, heavy elements disintegrate due to the high entropy per nucleon. This leads to the production of light nuclei, such as n, p, and  $^4\text{He}$ . Usually, the final chemical composition is not in chemical equilibrium, and depends on the time variation of  $\rho$  and  $T$  after passage of the shock wave.

Here, we focus on the death of a star having  $\sim 20M_{\odot}$  in the main-sequence stage, like SN 1987A. In this case, the mass cut is assumed to be located in the Si-rich layer of the progenitor. Hence, we explain the explosive nucleosynthesis in the Si-rich layer and O-rich layer, where explosive nucleosynthesis in our interest occurs.

#### (i) Explosive Si-burning

In the explosive Si-burning layer of  $T \approx 5 \times 10^9\text{K}$ , an alpha-rich freezeout occurs. After passage of the shock wave, most nuclei are at first photo-disintegrated. Then, nuclei begin to recombine with each other as the temperature falls along with expansion. At such a high temperature, all of the Coulomb barriers can be overcome, and Fe-group nuclei are mainly synthesized. It should be noted that how the produced elements are neutron rich is very sensitive to the distribution of  $Y_e$  in the Si-rich layer, which is formed during the silicon shell-burning stage. For an electron fraction of  $Y_e \geq 0.493$  the most abundant nucleus is the doubly-magic nucleus  $^{56}\text{Ni}$ , which has the largest binding energy per nucleon for  $N = Z$ . On the other hand, if  $Y_e < 0.493$ , the most abundant nucleus becomes  $^{58}\text{Ni}$ . Important radioactive nuclei,  $^{57}\text{Ni}$  and  $^{44}\text{Ti}$ , which are sources of heating the ejecta, are also synthesized in this layer.

#### (ii) Explosive O-burning

At the inner-most region of the O-rich layer, the peak temperature becomes sufficiently high to produce Fe-group nuclei. The important thing to be emphasized is that  $Y_e$  is nearly 0.5 in this layer, because electron capture does not work effectively during the oxygen shell burning stage. As a result, it is not  $^{58}\text{Ni}$ , but  $^{56}\text{Ni}$ , that is produced mainly at the inner most region of the O-rich layer.

As the shock wave decays, Fe-group nuclei cannot be produced through explosive burning because of the bottle neck at the proton magic number  $Z = 20$ . A temperature larger than  $\sim 3.3 \times 10^9$  K leads to a quasi-statistical equilibrium (QSE) among nuclei in the range  $28 < A < 45$  in mass number.

## 2.2. Observational Data

It is only SN 1987A in the Large Magellanic Cloud that has provided the most precise data to prove the validity of explosive nucleosynthesis calculations. For example, the mass of  $^{56}\text{Ni}$  has been estimated to be  $0.07\text{--}0.076M_\odot$  on the basis of a luminosity study (Shigeyama et al. 1988; Woosley, Weaver 1988). The values of  $\langle^{57}\text{Ni}/^{56}\text{Ni}\rangle$  and  $\langle^{58}\text{Ni}/^{56}\text{Ni}\rangle$  are also determined from the observation. These values are defined as below:

$$\langle^{57}\text{Ni}/^{56}\text{Ni}\rangle \equiv [X(^{57}\text{Ni})/X(^{56}\text{Ni})]/[X(^{57}\text{Fe})/X(^{56}\text{Fe})]_\odot,$$

$$\langle^{58}\text{Ni}/^{56}\text{Ni}\rangle \equiv [X(^{58}\text{Ni})/X(^{56}\text{Ni})]/[X(^{58}\text{Ni})/X(^{56}\text{Fe})]_\odot,$$

where  $X$  denotes the mass fraction. The ratio of  $^{57}\text{Ni}$  to  $^{56}\text{Ni}$  has been determined from the X-ray light curve to be  $1.5 \pm 0.5$  times the solar  $^{57}\text{Fe}/^{56}\text{Fe}$  ratio (Kurfess et al. 1992). From the spectroscopic observation of SN 1987A, the mass of  $^{58}\text{Ni}$  in SN 1987A has been estimated to be  $\sim 0.0022\text{--}0.003M_\odot$  (Rank et al. 1988; Witterborn et al. 1989; Aitken et al. 1988; Meikle et al. 1989; Danziger et al. 1991), which gives the ratio  $\langle^{58}\text{Ni}/^{56}\text{Ni}\rangle \sim 0.7\text{--}1.0$ . In section 4, we will present the initial conditions of the shock wave that satisfy these three observational constraints.

## 3. Models and Calculations

### 3.1. Hydrodynamics and Nuclear Reaction Network

In this section we explain our numerical calculation method. We performed 1-dimensional hydrodynamical calculations. The number of meshes is 300 in the radial direction. The inner and outer most radius are set to be  $10^8$  cm and  $2 \times 10^{10}$  cm, respectively. We adopt the Roe method for the calculation (Roe 1981; Yamada, Sato 1994). We use the equation of state;

$$P = \frac{1}{3}aT^4 + \frac{\rho k_B T}{A_\mu m_u}, \quad (1)$$

where  $a$ ,  $k_B$ ,  $A_\mu$ , and  $m_u$  are the radiation constant, the Boltzmann constant, the mean atomic weight, and the atomic mass unit, respectively.

We also use a test-particle method to see the variations of  $(\rho, T)$  in the Lagrangian coordinate. Let us explain this method. It is assumed that test particles are at rest in the beginning and move with the local velocity at their positions after the passage of a shock wave. We can thus calculate each particle's path by integrating  $\frac{d\vec{x}}{dt} = \vec{v}(t, \vec{x})$ , where the local velocity  $\vec{v}(t, \vec{x})$  is given from the hydrodynamical calculations mentioned above. The density and temperature of a test particle at each time step are obtained through an interpolation between the Eulerian meshes where the particle is found at the moment. We can thus obtain information about  $(\rho, T)$  for the Lagrangian coordinate, while preserving the time variation of the density and temperature along each trajectory of the test particles.

Next, we calculate the explosive nucleosynthesis using the time-dependent data of  $(\rho, T)$ . Since the system is not in chemical equilibrium, we must calculate the change in the chemical composition using a nuclear reaction network containing 242 nuclear species (see figure 1., Hashimoto et al. 1989).

It is noted that we assume that the system is adiabatic after the passage of a shock wave, because the entropy produced during explosive nucleosynthesis is much smaller than that generated by the shock wave. Thus, nucleosynthesis calculations are carried out separately, so-called *post processing*, for each trajectory of the test particles using the nuclear reaction network. Refer to Nagataki et al. (1997) for details concerning the numerical method, which has also been used in a calculation of asymmetric explosive nucleosynthesis.

### 3.2. Initial Condition

The progenitor of SN 1987A, Sk  $-69^\circ 202$ , is thought to have had the mass of  $\sim 20M_\odot$  in the main-sequence stage (Shigeyama et al. 1988; Woosley, Weaver 1988) and had an  $\sim (6\pm 1)M_\odot$  helium core (Woosley 1988). We used the presupernova model just before the collapse obtained from the evolution of a helium core of  $6 M_\odot$  (Nomoto, Hashimoto 1988) as the initial model for density and compositions. We stress that calculations were performed while keeping the original distribution of  $Y_e$ . Table 1 shows the radii of the Fe/Si, Si/O, and O/He interfaces in this model, where a discontinuity of the compositions exists due to convective shell burning.

We now explain the way that the shock wave is initiated in this study. We deposit some amount of energy (input

energy) as a combination of the internal energy and kinetic energy at the inner-most edge of the calculation region. Both the internal energy and the initial velocity are assumed to be proportional to the radius. Although the way of injecting the explosion energy is artificial, we note that the velocity of the Sedov solution in uniform density is proportional to the radius (Sedov 1959). The initial velocity is also assumed to be radial. The input energy is set to be  $2.0 \times 10^{51}$  erg (2 foes), which is appropriate for SN 1987A, since the final explosion energy, 1 foe, is the sum of the input energy and the gravitational binding energy above the mass cut. The ratio of the internal energy to the kinetic energy is changed parametrically to see its effect on the nucleosynthesis. We also studied the effect of a change in the range of the region where the input energy is injected. We note that locating the input energy further away from the center implies setting the final explosion energy larger. The initial conditions explored in this study are summarised in table 2.

#### 4. Results

As stated in section 3, the initial shock waves of models Cs (Ca–Cc) are strongest and those of As (Aa–Ac) are weakest. In this section we consider the results of the intermediate strength of the shock waves, that is, the results of Bs (Ba–Bc) for representation. In particular, we discuss models Ba and Bc in order to understand the effect of the ratio of the initial kinetic energy to the initial thermal energy. The products from explosive nucleosynthesis depend crucially on the peak temperature, which is affected by the method of shock initiation. To see the difference of  $(\rho, T)$  during shock-wave propagation, we show in figure 2. changes in  $(\rho, T)$  with time for a test particle initially placed at the boundary between the O-rich and Si-rich layer ( $r = 3.0 \times 10^8$  cm) for models Ba and Bc. We can see that the peak temperature is higher in model Bc at  $t \sim 0.04$  s than that in model Ba at  $t \sim 0.06$  s. To see this tendency more clearly, we show the peak temperature for models Ba and Bc in figure 3.. The abscissa represents the initial position of each test particle. We can see that the peak temperature is higher at first ( $r < 1.8 \times 10^8$  cm) in model Ba. On the other hand, the peak temperature of model Bc is higher in the rest of the region. We can give an explanation to this phenomenon as follows. The temperature is simply determined by the internal-energy density behind the shock wave, because this region is photon-dominated. Since the input energy is deposited only in the form of internal energy, the peak temperature becomes higher at first in model Ba. However, as the shock wave proceeds forward, the shock becomes weaker compared that in model Bc, since more energy is dissipated at smaller

radii. As a result, the peak temperature of model Ba becomes lower for  $r > 1.8 \times 10^8$  cm compared with model Bc. This tendency is consistent with the result of Aufderheide et al. (1991) as can be seen from their figure 7.

We now examine the effect on explosive nucleosynthesis. We calculated the total amount of heavy elements in the range  $A = 16-73$  and compared them with the solar system abundances. Some comments are necessary concerning this analysis. First, all unstable nuclei produced were assumed to decay to stable ones when compared with the solar values. Second, the mass cut was determined so as to contain  $0.07M_{\odot}$  of  $^{56}\text{Ni}$  in the ejecta. The mass cut for each model is shown in table 3 along with the peak temperature at the Si/O interface. We also note that the initial mass function (IMF), the chemical composition in the ejecta for each mass of the progenitors, and the ratio of Type I to Type II supernova are necessary when a comparison with the solar-system abundances is made in relation to the chemical evolution of the galaxy. In the present investigation, we can only see to what extent the abundances could be affected by the form of the initial shock wave.

Figures 4. and 5. show the results for models Ba and Bc. The former shows a comparison of the composition for  $A = 16-73$  between models Ba and Bc. The dots denote the mass fraction ratio of model Bc to Ba. The latter illustrates a comparison of the abundances of ejected nuclei with the solar values (normalized at  $^{16}\text{O}$ ). The open circles represent Ba/Solar and the dots correspond to Bc/Solar, respectively. It is evident from figure 4. that the number of nuclei in the range  $A = 16-50$  is almost the same between the two models and within a factor of 2-3 in the range  $A = 50-73$ . Therefore, the ratios  $\langle^{57}\text{Ni}/^{56}\text{Ni}\rangle$  and  $\langle^{58}\text{Ni}/^{56}\text{Ni}\rangle$  are subject to a considerable change in our models.

We show in table 4 the ratios  $\langle^{57}\text{Ni}/^{56}\text{Ni}\rangle$  and  $\langle^{58}\text{Ni}/^{56}\text{Ni}\rangle$  for all the models. We can see the tendency that the ratios  $\langle^{57}\text{Ni}/^{56}\text{Ni}\rangle$  and  $\langle^{58}\text{Ni}/^{56}\text{Ni}\rangle$  become smaller as the ratio of the initial kinetic energy to the internal energy becomes larger. The reason can be explained as follows. The peak temperature reaches becomes in a model which has more kinetic energy initially, and  $^{56}\text{Ni}$  is more produced in the O-rich layer. Therefore, the mass cut must be taken larger in its size compared with the bomb method, and neutron-rich elements, such as  $^{57}\text{Ni}$  and  $^{58}\text{Ni}$ , are less included in the ejecta. To clarify this explanation, we show in figure 6. the mass fraction of  $^{56}\text{Ni}$  and  $^{58}\text{Ni}$  for models of Ba and Bc. It is evident that  $^{56}\text{Ni}$  is synthesized more in the outer region in model Bc compared with model Ba. Additionally, we can see the tendency that the abundance ratios are smaller, since the energy-deposition region is assumed to be smaller and to be located farther away from the center. This is so for the same reason as mentioned above. As a consequence, the ratios of  $\langle^{57}\text{Ni}/^{56}\text{Ni}\rangle$  and  $\langle^{58}\text{Ni}/^{56}\text{Ni}\rangle$  are near to the range of the observational

uncertainty for model Cc, even if the  $Y_e$  distribution of the progenitor is not changed artificially.

We comment on the total mass of  $^{56}\text{Ni}$  synthesised in the O-rich layer. In this layer, electron capture hardly occurs, contrary to the case in the Si-rich layer. If  $^{56}\text{Ni}$  is synthesised mainly in the O-rich layer, the treatments of electron capture and convection are less important concerning the outcome of explosive nucleosynthesis. As can be seen in table 4, most of the  $^{56}\text{Ni}$  is synthesized in the O-rich layer in model Cc.

## 5. Summary and Discussion

We have carried out 1-dimensional calculations using various initial conditions in order to determine its influence on explosive nucleosynthesis. We find a tendency that the peak temperature becomes higher if the input energy is deposited more in the form of kinetic energy than that of the internal energy, because this makes the mass cut larger; neutron-rich matter is less included in the ejecta, which is good for reproducing the observational data. We must only say that a fairly strong initial shock-wave, like model Cc, must be assumed for reproducing the observation  $\langle^{58}\text{Ni}/^{56}\text{Ni}\rangle$ , to be sure.

Since there is no reason why the input energy is deposited in the form of either internal energy or kinetic energy alone, it will be very favorable to find that some combinations of them can reproduce the observational data with the electron fraction of the progenitor unchanged. In other words, our conclusion is that treatments of the various processes for stellar evolution, such as convection and electron capture during the silicon burning stage, are still compatible with the results of explosive nucleosynthesis calculations. Then, the condition for the initial shock wave in our models should be the outcome of the core-collapse, the bounce, and shock-wave propagation from the central region. In particular, the demand concerning the amount of kinetic energy at the Si-rich layer may be a strong constraint for the model of a delayed explosion, because in that model the shock wave stalls at first and is revived by neutrino heating, which may result in a low ratio of the kinetic energy to the thermal energy.

We note the astrophysical implications of our results. First, the central compact object could be a pulsar for all our models, since the mass cut is below the upper limit of the neutron- star mass, even in the case of Cc. However, there is also the possibility to generate a more massive accretion disk around a neutron star for a larger mass cut. This means that the central compact system has more activity in the larger mass cut case. Secondly, more radioactive nuclei will be included in the compact object if they survive there. This also shows a higher activity

at the central compact system, as suggested by Mineshige et al. (1992). In particular, these effects lead to the emission of gamma-rays, which could contribute to the observation of the supernova remnant. To say conversely, the observation of gamma-rays from a pulsar and its accretion disk may be a touchstone of our results. Finally, we note the uncertainty of the abundance of nuclei in the range  $A = 50\text{--}73$ . Since the solar-system abundances of the heavy elements  $A \geq 50$  are generated mainly by Type Ia supernova (Tsujimoto et al. 1995), this uncertainty may be less stressed. However, we believe that we must keep this uncertainty in mind when an individual collapse-driven supernova is observed and analyzed.

We comment on the hydrodynamical code. Though our code is Eulerian and that of Aufderheide et al. (1991) is Lagrangian, our results are consistent with theirs. Therefore, our conclusions that the peak temperature becomes higher, the mass cut becomes larger, and neutron-rich matter is less included in the ejecta do not depend on the hydrodynamical scheme. Therefore, we believe that the uncertainty of the initial condition discussed in the present research should be kept in mind when studying explosive nucleosynthesis, and that it would help to solve the problem concerning the overproduction of neutron-rich matter for some progenitor models.

This research has been supported in part by a Grant-in-Aid for the Center-of-Excellence (COE) Research (07CE2002) and for the Scientific Research Fund (05243103, 07640386, 3730) of the Ministry of Education, Science, Sports and Culture in Japan. and by Japan Society for the Promotion of Science Postdoctoral Fellowships for Research Abroad.

**References**

- Aitken D.K., Smith C.H., James S.D., Roche P.F., Hyland A.R., McGregor P.J. 1989, MNRAS 235, 19
- Arnett W.D. 1996 *Supernova and Nucleosynthesis* (Princeton University Press, Princeton) chapter 9
- Aufderheide M.B., Baron E., Thielemann F.K. 1991, ApJ 370, 630
- Danziger I.J., Lucy L.B., Bouchet P. 1991 in *Supernovae*, ed S.E. Woosley (Springer, Berlin)p69
- Fuller G.M., Fowler W.A., Newman M. 1980, ApJS 42, 447
- Fuller G.M., Fowler W.A., Newman M. 1982, ApJS 48, 279
- Hashimoto M. 1995, Prog. Theor. Phys. 94, 663
- Hashimoto M., Nomoto K., Shigeyama T. 1989, A&A 210, L5
- Kurfess J.D., Johnson W.N., Kinzer R.L., Kroeger R.A., Strickman M.S., Grove J.E. 1992, ApJ 399, L137
- Meikle W.P.S., Allen D.A., Spyromilio J., Varani G.-F. 1989, MNRAS 238, 193
- Mineshige S., Nomoto K., Shigeyama T. 1992, A&A 267, 95
- Nagataki S., Hashimoto M., Sato K., Yamada S. 1997, ApJ 486, 1026
- Nomoto K., Hashimoto M. 1988, Phys. Rep. 163, 13
- Rank D.M., Pinto P.A., Woosley S.E., Bregman J.D., Witterborn F.C., Axelrod T.S., Cohen M. 1988, Nature 331, 505
- Roe P.L. 1981 J. Comput. Phys. 43, 357
- Sedov L.I. 1959, *Similarity and Dimensional Methods in Mechanics* (Academic Press, New York) chapter 4
- Shigeyama T., Nomoto K., Hashimoto M. 1988, A&A 196, 141
- Thielemann F.-K., Hashimoto M., Nomoto K. 1990, ApJ 349, 222
- Tsujimoto T., Nomoto K., Hashimoto M., Thielemann F.-K. 1994, in *Evolution of the Universe and its Observational Quest*, ed K. Sato (Universal Academy Press, Tokyo) p553
- Witterborn F.C., Bregman J.D., Wooden D.H., Pinto P.A., Rank D.M., Woosley S.E., Cohen M. 1989, ApJ 338, L9
- Woosley S.E. 1988, ApJ 330, 218
- Woosley S.E., Weaver T.A. 1988, Phys. Rep. 163, 79
- Woosley S.E., Weaver T.A. 1995, ApJS 101, 181
- Yamada S., Sato K. 1994, ApJ 434, 268

Table 1. Radius of the interface for each layer.

Interface	Radius [cm]	Radius [ $M_{\odot}$ ]
Fe/Si	$1.5 \times 10^8$	1.4
Si/O	$3.0 \times 10^8$	1.7
O/He	$6.3 \times 10^9$	3.8

Table 2. Initial conditions and name of each model.

$E_{\text{kin}} : E_{\text{th}}^*$	$R_{\text{inp}}/10^8 \text{cm}^{\dagger}$		
	1.0–1.5	1.4–1.5	1.9–2.0
0% : 100%	Aa	Ba	Ca
30% : 70%	Ab	Bb	Cb
70% : 30%	Ac	Bc	Cc

\* The ratio of the initial kinetic energy to the internal energy.

† The radius ( $10^8$  cm) where the input energy is deposited.

Table 3. Mass cut and peak temperature at Si/O interface for each model.

Model	Mass cut ( $M_{\odot}$ )	Mass cut (cm)	Temperature (K) at Si/O
Aa	1.54	$1.97 \times 10^8$	$4.8 \times 10^9$
Ab	1.57	$2.13 \times 10^8$	$5.2 \times 10^9$
Ac	1.58	$2.21 \times 10^8$	$5.4 \times 10^9$
Ba	1.56	$2.07 \times 10^8$	$5.3 \times 10^9$
Bb	1.59	$2.28 \times 10^8$	$5.5 \times 10^9$
Bc	1.60	$2.34 \times 10^8$	$5.8 \times 10^9$
Ca	1.60	$2.33 \times 10^8$	$5.9 \times 10^9$
Cb	1.61	$2.43 \times 10^8$	$6.3 \times 10^9$
Cc	1.63	$2.56 \times 10^8$	$6.6 \times 10^9$

Table 4. The ratios of  $\langle^{57}\text{Ni}/^{56}\text{Ni}\rangle$  and  $\langle^{58}\text{Ni}/^{56}\text{Ni}\rangle$  for each model.

Model	$\langle^{57}\text{Ni}/^{56}\text{Ni}\rangle$ ( $1.5 \pm 0.5$ )	$\langle^{58}\text{Ni}/^{56}\text{Ni}\rangle$ (0.7–1.0)	Mass of $^{56}\text{Ni}$ in O-layer
Aa	2.7	9.0	$5.6 \times 10^{-3} M_{\odot}$
Ab	2.3	6.6	$2.3 \times 10^{-2} M_{\odot}$
Ac	2.1	5.7	$2.9 \times 10^{-2} M_{\odot}$
Ba	2.3	6.2	$1.7 \times 10^{-2} M_{\odot}$
Bb	1.9	3.8	$3.3 \times 10^{-2} M_{\odot}$
Bc	1.8	3.0	$3.8 \times 10^{-2} M_{\odot}$
Ca	2.1	4.6	$4.0 \times 10^{-2} M_{\odot}$
Cb	2.0	3.5	$4.7 \times 10^{-2} M_{\odot}$
Cc	1.6	1.3	$5.6 \times 10^{-2} M_{\odot}$

The values in the parentheses mean the observational values. The last column denotes the total mass of  $^{56}\text{Ni}$  synthesized in O-rich layer.

## Figure Captions

Fig. 1. Table of nuclei included in our nuclear reaction network; 242 species are included. The gray-colored nuclei denote stable nuclei.

Fig. 2. Time variation of  $(\rho, T)$  for the test particle, which is located at  $r = 3.0 \times 10^8$  cm. The dashed line is for model Ba and the solid line is for model Bc.

Fig. 3. Peak temperature of models Ba and Bc. The abscissa means the initial position of each test particle. The dashed line is for model Ba and the solid line is for model Bc.

Fig. 4. Comparison of the composition for the mass number range  $A = 16-73$  between models Ba and Bc.

Fig. 5. Comparison of the abundance of each nucleus with the solar value (normalised to  $^{16}\text{O}$ ). The open circles and solid points correspond to Ba/solar and Bc/solar, respectively.

Fig. 6. Final mass fraction of  $^{56}\text{Ni}$  and  $^{58}\text{Ni}$  for models Ba and Bc. The radius means the initial radius of the progenitor.

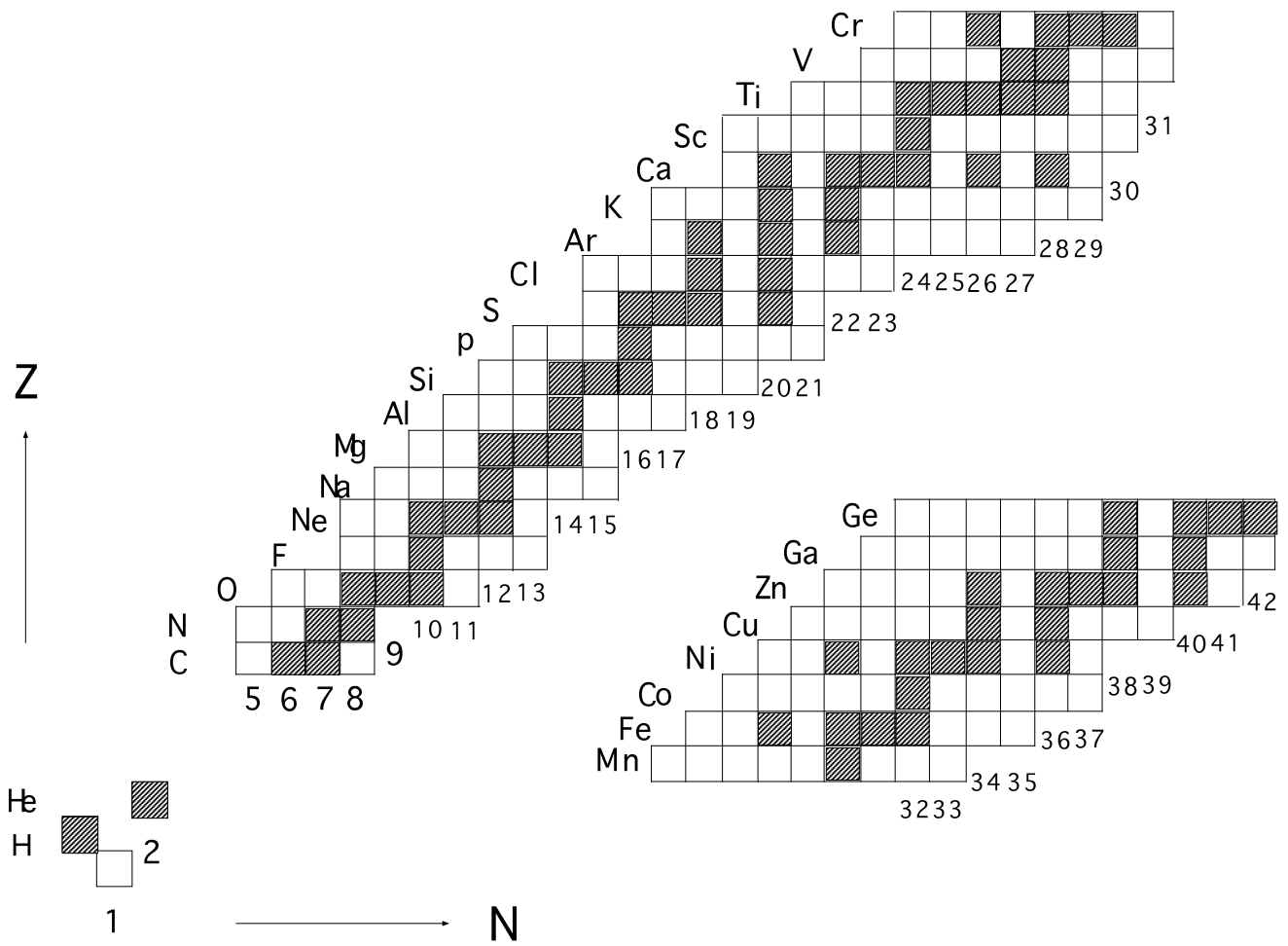


Fig. 1.

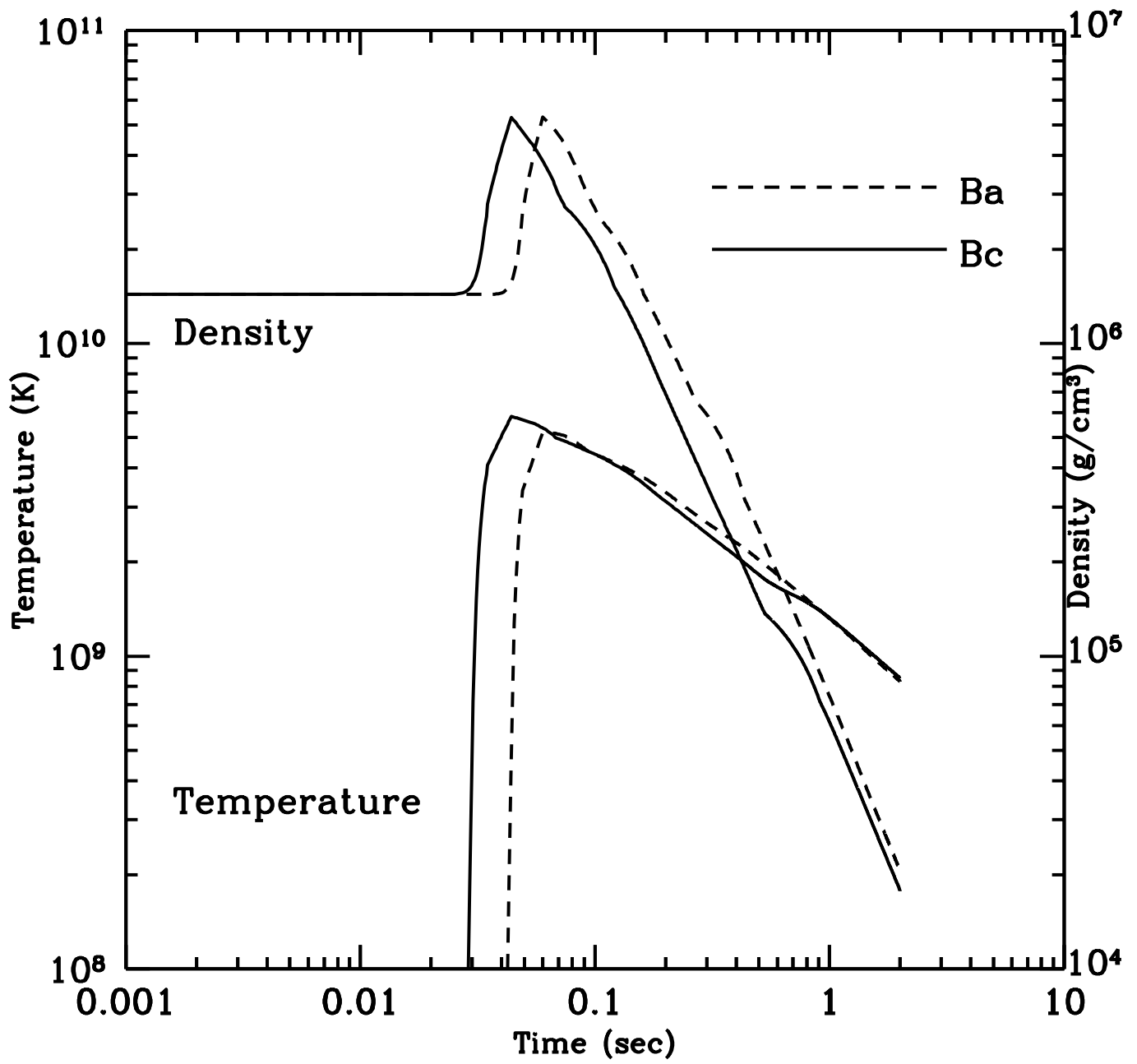


Fig. 2..

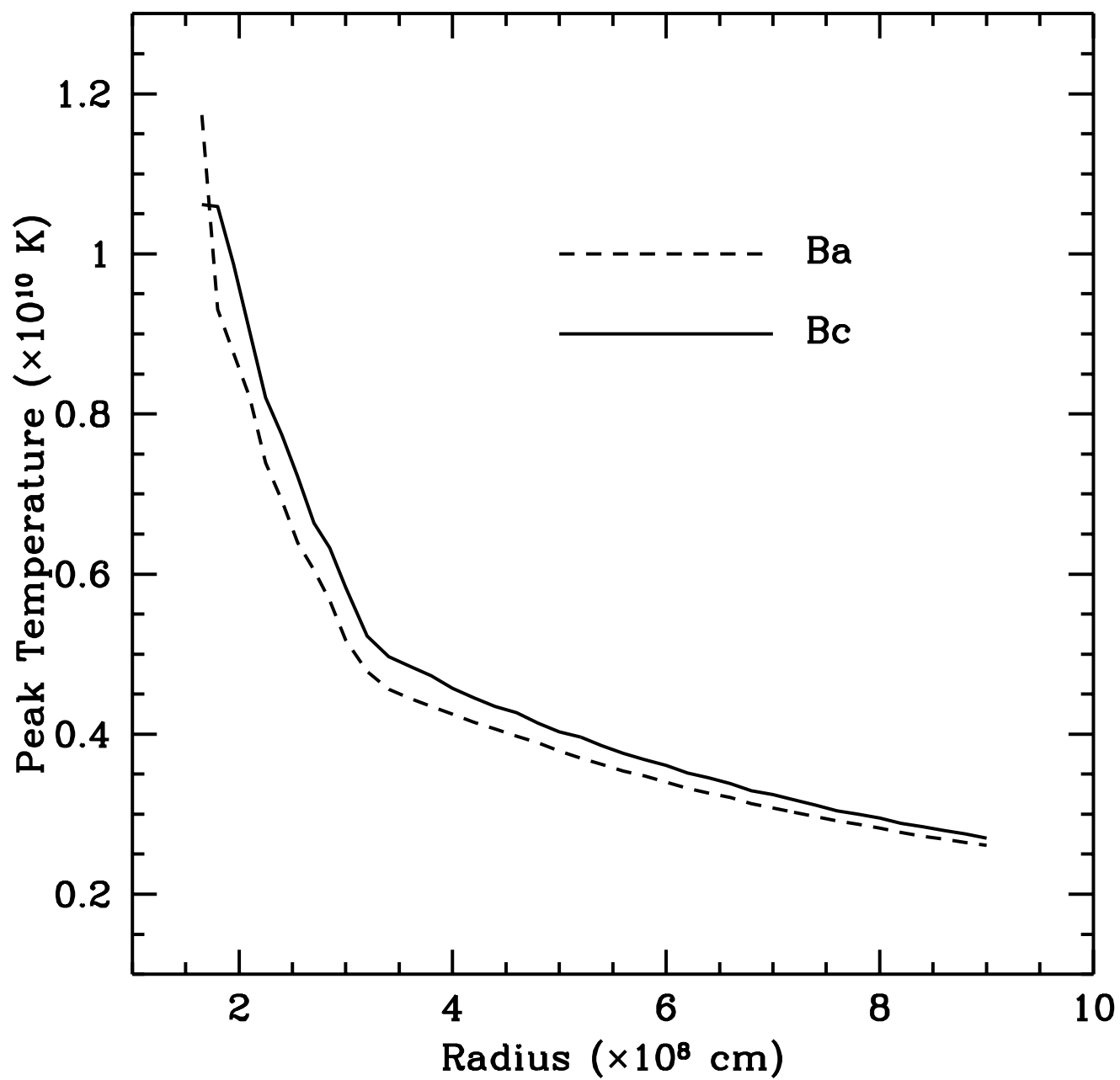


Fig. 3..

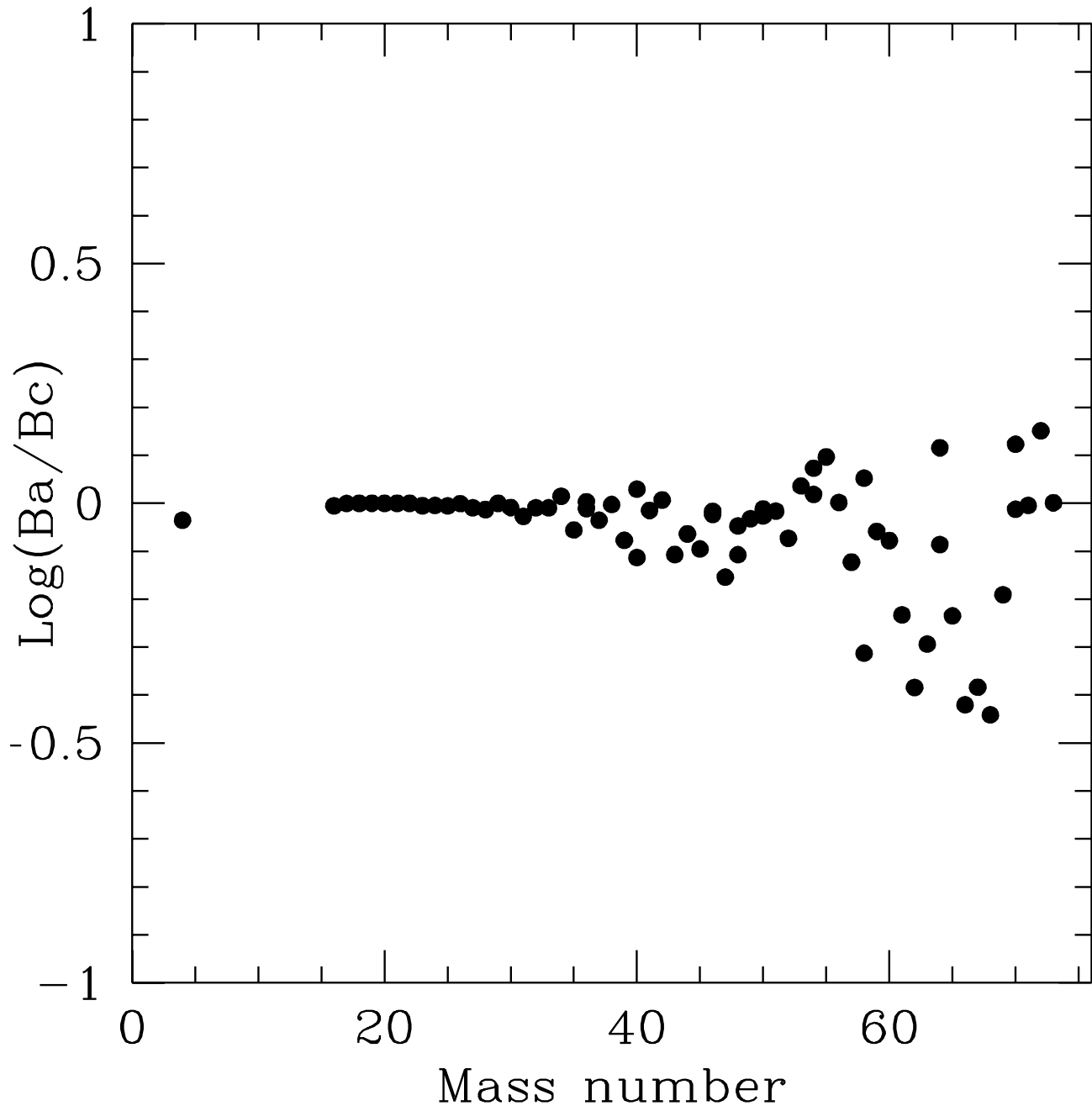


Fig. 4..

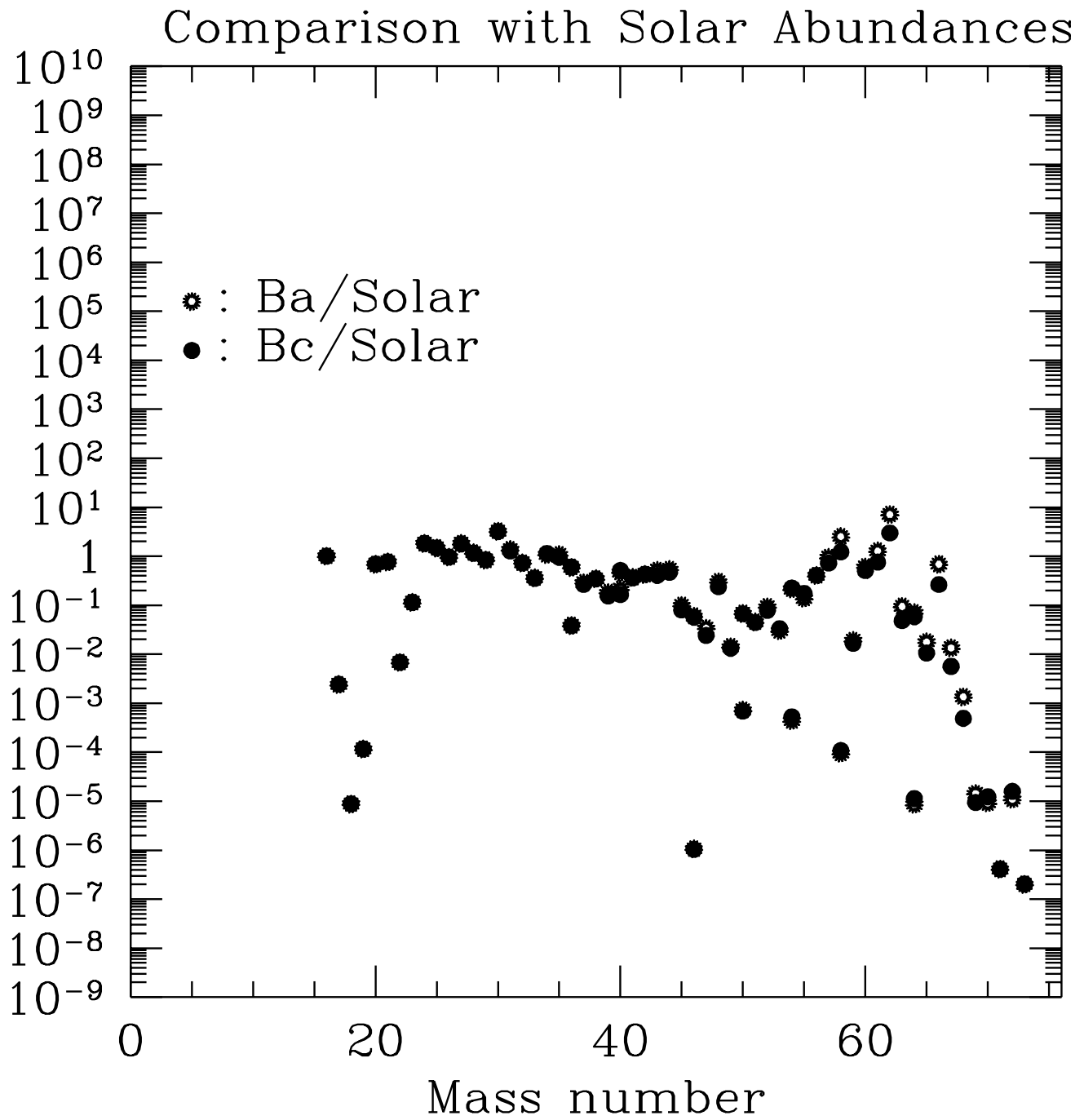


Fig. 5..

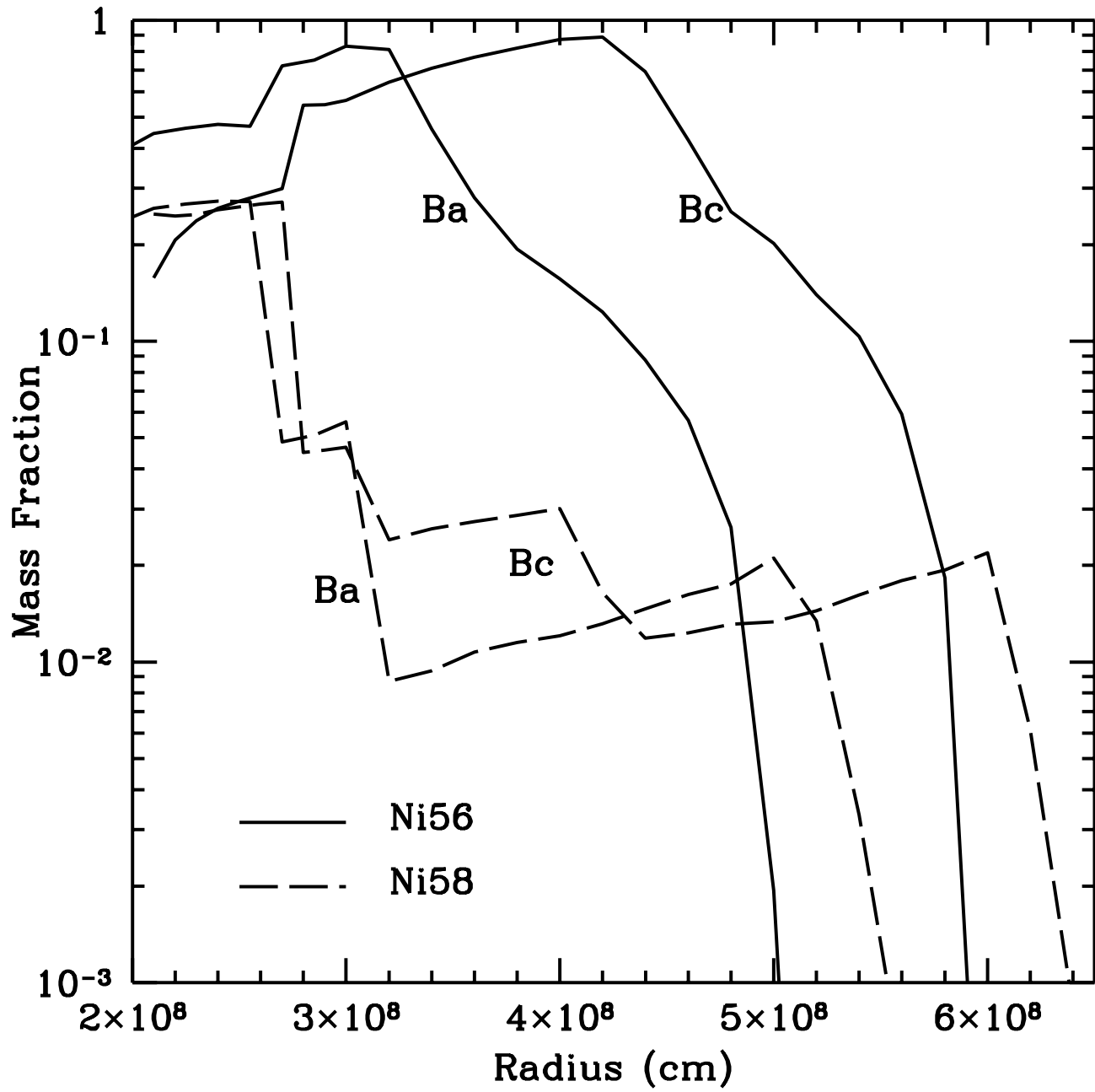


Fig. 6..